Robust Biocomposite Film of Polylactic Acid and Ferroferric Oxide as a Radar Absorbing Material

Rafles Sinaga[1], Wida Banar Kusumaningrum[2], Yana Taryana[3], Widya Fatriasari[2], Zuratul Ain Abdul Hami[4], Lisman Suryanegara[2*], Holilah Holilah[2], and Yudi Darma[1]**

[1]*Department of Physics, Faculty of Mathematics and Natural Sciences, Institut Teknologi Bandung, Jl. Ganesha No. 10, Bandung 40132, Indonesia*

[2]*Research Center for Biomass and Bioproducts, National Research and Innovation Agency, Cibinong 16911, Indonesia*

[3]*Research Center for Electronics and Telecommunication, National Research and Innovation Agency, Bandung 40135, Indonesia*

[4]*School of Materials & Mineral Resources Engineering, Universiti Sains Malaysia, Nibong Tebal Pulau Pinang 14300, Malaysia*

* ***Corresponding author:***

email: lisman.suryanegara@brin.go.id; yudi@itb.ac.id***

Received: November 11, 2022
Accepted: March 6, 2023

DOI: 10.22146/ijc.79089

Abstract: *The polymer/ferroferric oxide (Fe_3O_4) foam and aerogel composites generally exhibit superior radar absorptivity performance. However, these composites have poor mechanical and thermal properties. This study manufactured a polylactic acid (PLA)/Fe_3O_4 bio-composite and evaluated the radar absorptivity, thermal, and mechanical properties of radar-absorbing material. The composites were prepared using a solvent casting method to mix PLA and Fe_3O_4 at varying concentrations, followed by evaporation, oven drying, and hot pressing into a film. Thermogravimetric analysis showed that the decomposition temperature of the PLA/Fe_3O_4-5% composite occurred at around 306 °C, which shifted to a lower decomposition temperature of PLA. The addition of 25 wt.% Fe_3O_4 improved the tensile modulus of neat PLA from 2.92 to 3.55 GPa. The vector network analyzer demonstrated that the addition of Fe_3O_4 at 25% improved the reflection loss of PLA from −5.17 to −25.83 dB at a thickness of 3 mm, with energy absorbed by 99.74% at frequency position 10.58 GHz. These results demonstrated that PLA/Fe_3O_4 composites have great potential in radar-absorbing practical applications.*

Keywords: *radar absorptivity; thermal properties; mechanical properties; reflection loss; PLA/Fe_3O_4 biocomposites*

■ INTRODUCTION

Nowadays, radar absorbing materials (RAM) have been massively developed in military equipment stealth applications to minimize reflected electromagnetic waves to the radar system [1-2]. Therefore, RAM, with its high absorptivity, ultra-thin, superior tensile strength, and good thermal stability, has attracted considerable research interest [3-4]. The basic principle of microwave absorption is to convert microwave energy into heat energy through various absorption mechanisms. Microwave absorbers were generally manufactured from carbon-based materials, conductive polymer-based materials, ceramics, and magnetic materials [5]. Various composites, including solid films, foams, and aerogels, were designed to enhance the absorptivity performance of radar waves. Foam or aerogel is one of the lightest materials because it is filled with air in the pores or internal cavities, generally prepared through freeze drying [6].

Ferroferric oxide (Fe_3O_4) is a magnetic material with excellent permeability and complex permittivity, the parameters that govern the significance of microwave absorption. Other advantages of Fe_3O_4 are high saturation magnetization value, high curie temperature, facile synthesis, and low cost [7-8]. Recently, researches have been directed toward increasing the microwave absorption of pure Fe_3O_4 particles, mainly based on particle sizes, including micro-spheres [9], nano-spheres [10], and nanocrystals

[11]. The Fe_3O_4 micro-sphere synthesized by a simple chemical at 90 °C showed a reflection loss value of –45.2 dB at 4.67 GHz; meanwhile, Fe_3O_4 nano-spheres and nanocrystals each showed a reflection loss (RL) of –21.2 dB at 5.6 and 8.16 GHz. However, Fe_3O_4 as an absorbent material has some limitations, including a rapid decrease in the value of the permeability at microwave frequencies, large density, ease of oxidation, and impedance mismatch, which hinders the effective performance of microwave absorbers [12].

The radar absorptivity performance of foam and aerogel composites manufactured from Fe_3O_4 dispersion in a polymer matrix has been evaluated in several previous studies. The foam and aerogel composites showed higher radar absorption values, low density, and good flexibility. Phadtare et al. [13] reported superior radar absorption performance of a Fe_3O_4/divinylbenzene/ethyl hexyl acrylate foam composite with an RL value of –23 dB at 9.3 GHz frequency position in 15 wt.% Fe_3O_4 filler concentration. In another study, Jiang et al. reported an RL value of –26.45 dB for the melamine/Fe_3O_4 foam composite at the frequency of 7.76 GHz with a filler ratio of 30 wt.% [14]. The large internal cavity will cause multi-reflection and polarization loss; therefore, more radar energy is trapped in the composite. The large internal cavity provides a larger surface area, which facilitates impendence matching and polarization loss through multi-reflections, causing attenuation of the radar wave in the material. These foam and aerogel composites have limitations in a broader of applications.

Polylactic acid (PLA) is a bio-based polymer with excellent mechanical and thermal properties compared with synthetic polymers such as polyethylene. Notably, PLA is one of the most commonly used biopolymers for various applications because of its ease of processing [15]. PLA has been prepared with various types of inorganic fillers for numerous applications, one of which is to improve thermal and mechanical properties [16]. PLA is a biodegradable plastic that has great potential to replace petroleum-based fuel plastics due to its high stiffness and strength [17].

The objective of this study is to evaluate the radar absorptivity, thermal and mechanical properties of PLA/Fe_3O_4 composites. The composites were prepared by mixing PLA and 5 to 25 wt.% Fe_3O_4 by solvent casting. The radar absorption performance of PLA/Fe_3O_4 composites was evaluated using a Vector Network Analyzer (VNA). Meanwhile, the thermal and mechanical properties of the composites were determined using thermogravimetric analysis and a universal testing machine, respectively. In addition, the morphological, crystal structure, and magnetic properties of the film composite were also investigated using Scanning Electron Microscope (SEM), X-ray Diffraction (XRD), and vibrating sample magnetometer (VSM).

■ EXPERIMENTAL SECTION

Materials

PLA 4043D was supplied by Natureworks Co., Minnetonka, MN (USA). Dichloromethane (DCM, ≥ 99.0%), ammonia solution 25%, and iron (III) chloride hexahydrate ($FeCl_3 \cdot 6H_2O$) were purchased from Merck KGaA, Germany. Ferrous sulfate heptahydrate ($FeSO_4 \cdot 7H_2O$, ≥ 99.0%) was supplied by HiMedia Laboratories Pvt.Ltd., India.

Instrumentation

The surface morphology of Fe_3O_4, neat PLA, and PLA/Fe_3O_4 composites was observed under SEM (JEOL JSM-IT200, Japan) operating at 3.0 kV. The sample of Fe_3O_4 was gold-coated to improve conductivity before observation. The crystal structure of the samples was evaluated by XRD (Shimadzu 7000, Japan) with an X-ray tube of Cu operating at 30.0 mA and 40.0 kV. The XRD pattern of samples was recorded in the interval of 10° to 80° at a speed of 2°/min. The degree of crystallinity (X_c) is calculated using the formula [19]:

$$Xc = \frac{\text{area of crystalline peaks}}{\text{area of all peaks (crystalline + amorphous)}} \times 100\%$$

The thermal stability of neat PLA and PLA/Fe_3O_4 composites was evaluated using PerkinElmer TGA 4000, USA. The samples were immersed in a closed aluminum pan. Temperature programs were from 25 to 600 °C at a temperature increase speed of 10 °C/min under a nitrogen condition. The heating scan of the specimens was used to estimate thermal parameters such as

decomposition temperature (T_d), temperature for 50% weight loss (T_{50}), and residual weight (remaining Fe_3O_4 content) at 600 °C. A universal testing machine (Shimadzu AGS-X series 10kN, Japan) was used to investigate the mechanical properties of the samples. The tensile testing samples were fabricated using a mini-jet pro to obtain a dumbbell-shaped tensile bar (ASTM D638-14 type V). The sample gauge length, width, and thickness were approximately 30, 3, and 3 mm, respectively, measured by a caliper when gripped. The crosshead rate was set at 1 mm/min. All data on mechanical properties were recorded in the 5 measurements. The magnetic hysteresis loops were investigated by a vibrating sample magnetometer (VSM250 Dexing Magnet Ltd) with an applied magnetic field of 1 tesla under ambient temperature. The sample dimensions prepared were 5 × 5 × 1 mm (length-width-thick). The radar absorption of the samples was analyzed using the waveguide method at a frequency of 8.0 to 12.0 GHz using a vector network analyzer (VNA) Anritsu MS46322A, Japan, at room temperature. The sample, which measured 30 × 30 × 3 mm (length, width, thickness) was placed on the port and coated with a metal reflector. The complex permeability and air transmittance were measured to calibrate the instrument, which found results of μ'' = ε'' = 1 and μ' = ε' = 0. The reflection loss was calculated using line transmitting theory by adhering to the processes outlined in prior publications [20].

Procedure

The preparation of Fe_3O_4 particles was carried out following the procedure of the previous study [18]. A slight modification was made by extending the stirring time of 5.406 g (0.02 mol) $FeCl_3{\cdot}6H_2O$ and 2.701 g (0.01 mol) $FeSO_4{\cdot}7H_2O$ from 30 min to 2 h. PLA (described in Table 1) was dissolved in a beaker using DCM under stirring for 4 h. The Fe_3O_4 particles were added gradually to the PLA solution after the PLA was completely dissolved, and the stirring was kept going for another 4 h. The PLA/Fe_3O_4 mixture was poured and dispersed on trays, and the dichloromethane solvent was evaporated at ambient temperature for 12 h before oven drying for 8 h at 80 °C. The dried mixture was cut into small pieces of around 5 × 5 mm and hot-pressed at a temperature of 155 °C with a pressure of 50 MPa for 10 min to obtain a PLA/Fe_3O_4 composite film of 3 × 3 cm with various thickness.

Table 1. The composition of the samples

Sample name	Fe_3O_4 (g)	PLA (g)	DCM (mL)
Neat PLA	0	10	100
PLA/Fe_3O_4-5%	0.5	9.5	100
PLA/Fe_3O_4-10%	1.0	9.0	100
PLA/Fe_3O_4-15%	1.5	8.5	100
PLA/Fe_3O_4-20%	2.0	8.0	100
PLA/Fe_3O_4-25%	2.5	7.5	100

■ RESULTS AND DISCUSSION

Morphological Analysis

The morphology of Fe_3O_4 is shown in Fig. 1(a). The SEM image shows Fe_3O_4 is a microparticle with an irregular shape with an average size of fewer than 5 μm. The previous co-precipitation method produced similar findings [18]. In the Fe_3O_4 particle preparation process, several factors influence particle size and particle distribution: stirring speed, ambient temperature, and solution, the concentration of ammonia solution, and the Fe^{2+} and Fe^{3+} reagents used [21].

The fracture morphology of neat PLA and PLA/Fe_3O_4 composites observed using SEM is shown in Fig. 1(b-g). It can be seen from the figure that the pure PLA fracture surface is caused by the insoluble PLA portion and the appearance of pores due to DCM evaporation. The addition of more fillers results in the formation of agglomerates. Fe_3O_4 particles were visible in the fine-grained composite, which spread uniformly in the PLA matrix with a diameter smaller than 5 μm even in the Fe_3O_4 concentration of 25 wt.%. At 5 wt.% Fe_3O_4 concentration, there were no obvious cracks or holes on the fracture surface of the composite, which means that good interfacial interactions occur between the PLA matrix and Fe_3O_4 particles. With the addition of Fe_3O_4 concentration in the composite, the holes or cracks are more clearly visible, which means that the interfacial interaction is getting weaker.

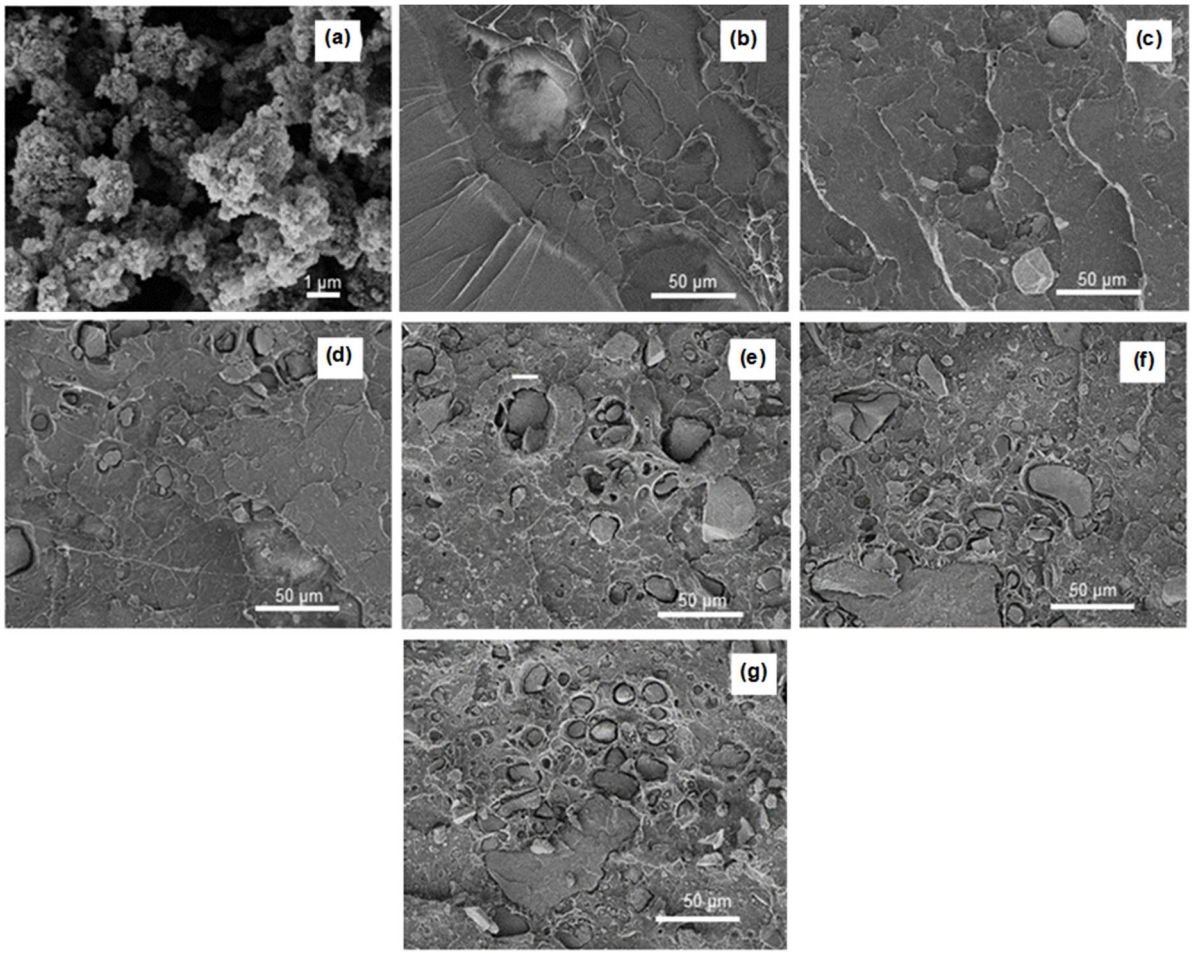

Fig 1. SEM images of morphology: (a) Fe_3O_4 particles; fracture of all composites: (b) Neat PLA, (c) PLA/Fe_3O_4-5%, (d) PLA/Fe_3O_4-10%, (e) PLA/Fe_3O_4-15%, (f) PLA/Fe_3O_4-20%, and (g) PLA/Fe_3O_4-25%

XRD Analysis

The diffraction peaks in the XRD pattern of Fe_3O_4, neat PLA, and PLA/Fe_3O_4 composites are shown in Fig. 2. The six diffraction peaks of Fe_3O_4 crystal at 2θ values are 30.3742, 35.6851, 43.3585, 53.8291, 57.5713, and 62.9956, according to the values of the index Miller of (220), (311), (400), (422), (511) and (440) crystal planes from the inverted cubic spinal structure of Fe_3O_4 (JCPDS 65-3107) [22-23]. These peaks indicated that the prepared Fe_3O_4 formed spinal structures, and no characteristic impurity peaks were detected in the XRD pattern.

Fig. 2 shows neat PLA exhibits large diffraction peaks at 2θ values of 16.52 and 32, which correspond to (200/110) and (203) according to a previous study [24]. When Fe_3O_4 particles were added, all composites displayed

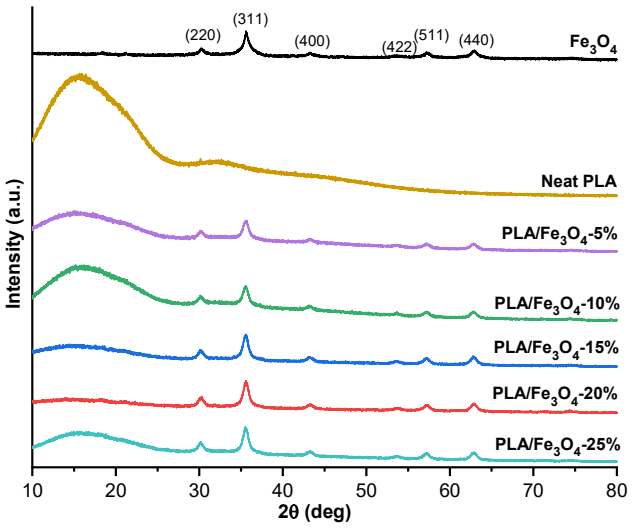

Fig 2. XRD patterns of Fe_3O_4, neat PLA, and PLA/Fe_3O_4 composites

broad diffraction peaks similar to the neat PLA peaks. The intensity of the PLA diffraction peaks did not increase with adding more Fe_3O_4 in the composite, although those shrunk and widened. The Fe_3O_4 addition may have prevented the development of numerous crystals and the organization of PLA molecular sequences, but it did not affect the crystal structure of PLA. Based on the calculation, X_c of neat PLA, PLA/Fe_3O_4-5%, PLA/Fe_3O_4-10%, PLA/Fe_3O_4-15%, PLA/Fe_3O_4-20%, and PLA/Fe_3O_4-25%, respectively, is 28.90, 32.69, 33.27, 34.48, 35.62, and 37.56%.

The Thermal Stability of PLA/Fe_3O_4 Composites

The TGA test was used to investigate the effect of Fe_3O_4 on the thermal stability of PLA. Fig. 3 shows the weight loss of PLA and PLA/Fe_3O_4 composites at varying Fe_3O_4 content as a function of temperature. The T_d, T_{50}, and residual Fe_3O_4 content at 600 °C are listed in Table 2. Based on the thermogram, we can see that neat PLA has thermal stability up to a degradation onset temperature of about 320 °C. Then, the decomposition temperature occurs at around 349 °C. After reaching it, the sample weight decreases drastically by a single-stage decomposition until the maximum rated temperature of 380 °C. The weight loss of the PLA continues to decrease slowly until the final test temperature, where the residual weight is 0.178%. The interactions between volatile organic compounds are primarily responsible for keeping the char structure firm. This thermal behavior is typical for polylactic acid polymers [25-26].

The presence of 10 wt.% Fe_3O_4 on the PLA could maintain thermal stability up to a temperature of 280 °C. The decomposition temperature of the PLA/Fe_3O_4-10% composite occurred at around 293 °C, which shifted to a lower decomposition temperature of PLA. Interestingly, the addition of a higher Fe_3O_4 concentration did not significantly change the decomposition temperature of the PLA composite. After the decomposition temperature, the weight of all composites dropped drastically until around 30 to 50% of the sample weight remained at 300 °C. The weight loss of the PLA composites continued decreasing slowly until the final test temperature. The visible changes were in the remaining weight of each composite, where the final weight was determined based on the concentration of Fe_3O_4. Considering the physicochemical properties and the chemical structure of the Fe_3O_4, it can be assumed that the observed reduction in thermal stability is related to two simultaneous mechanisms. A similar effect is observed in the case of thermal stability of the other PLA/inorganic-filler composites, where the presence of copper slag contributes to a reduction in the decomposition temperature of PLA [25].

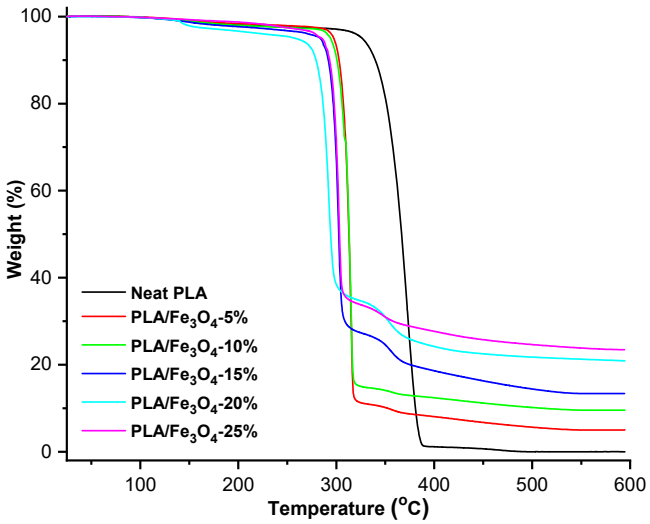

Fig 3. Thermogravimetric curves of neat PLA and PLA/Fe_3O_4 composites with different Fe_3O_4 contents (wt.%)

Table 2. TGA results of neat PLA and PLA/Fe_3O_4 composites

Samples	T_d (°C)	$T_{0.50}$ (°C)	Residual weight (%)
Neat PLA	349.16	365.13	0.178
PLA/Fe_3O_4-5%	306.14	312.92	5.020
PLA/Fe_3O_4-10%	304.23	312.36	9.707
PLA/Fe_3O_4-15%	297.14	303.32	13.390
PLA/Fe_3O_4-20%	258.23	288.22	20.896
PLA/Fe_3O_4-25%	295.85	302.41	23.355

The Mechanical Properties of PLA/Fe_3O_4 Composites

A tensile test was used to evaluate the influence of Fe_3O_4 addition on the mechanical characteristics of PLA. Table 3 and Fig. 4 present the mean and standard deviation of the mechanical properties of all the samples. The table and figure clearly show the tensile modulus of PLA improved with an increase of Fe_3O_4 content while the tensile strength and strain at break decreased. The addition of 5 wt.% Fe_3O_4 improved the modulus from 2.92 to 3.09 GPa. Furthermore, the composite stiffness increased significantly with the addition of a higher Fe_3O_4 concentration. The composite reached the highest stiffness of 3.55 GPa at a 25 wt.% Fe_3O_4 content.

It is clearly shown that added Fe_3O_4 deteriorated the composite strength compared to neat PLA. The decrease in tensile strength of PLA occurred after the addition of 5 wt.% Fe_3O_4 content from 67.57 to 57.94 MPa. Therefore, we could see that the strength remains almost constant between 5 to 25 wt.% Fe_3O_4 content. This decrease in the tensile strength of the composites was caused by poor interface adhesion between Fe_3O_4 particles and PLA. The weakened ion-dipole interaction between the ferrite cation and oxygen atom in the PLA carbonyl group also affects to decrease of tensile strength. The strain at the break value of neat PLA increased almost two times with the addition of 5% by weight of Fe_3O_4 from 3.52 to 5.21%. Then it decreased with the addition of Fe_3O_4 filler and reached 2.08% for 5 wt.% filler content. A decrease in elongation at break with the addition of Fe_3O_4 to polymers is commonly observed in thermoplastic composites. In brief, the mechanical properties of these composites depend on the following factors: the adhesion between the PLA matrix and the Fe_3O_4 filler, the ratio of the Fe_3O_4 filler to the PLA polymer, the size of the Fe_3O_4 filler, the type and characteristics of the filler, and the degree of crystallinity of the matrix [16]. Decreased interphase stress results in reduced bond strength of the polymer structure. In addition, low adhesion between the matrix and filler results in cavities at the filler matrix interface resulting in a change in the strength value [27]. The tensile modulus value describes the stiffness of a material that allows it to withstand loads without shape deformation. High tensile strength and modulus values are needed for large loads [28].

Magnetic Property Analysis of PLA/Fe_3O_4 Composites

The hysteresis loops of neat PLA and PLA/Fe_3O_4 composite are shown in Fig. 5(a). The magnetic properties such as saturation magnetization (M_s), remanence magnetization (M_r), and coercive field (H_c) are listed in Table 4. A magnet attraction test was performed to determine the magnetic response of neat PLA and PLA/Fe_3O_4 composite. Neat PLA has no response,

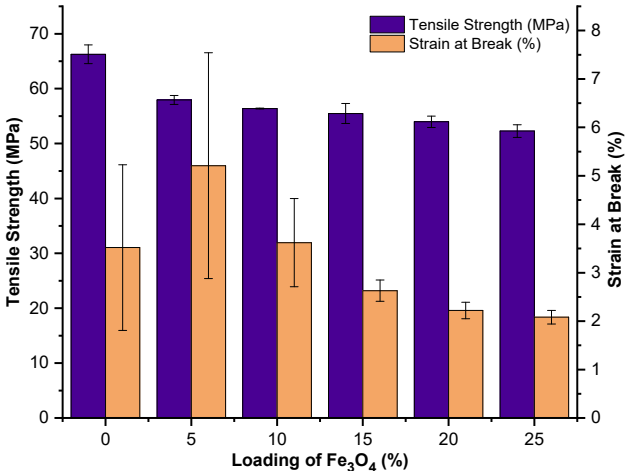

Fig 4. The graphs of tensile strength and strain at break depend on variations in Fe_3O_4 loading

Table 3. Mechanical properties of neat PLA and PLA/Fe_3O_4 composites

Samples	Tensile modulus (GPa)	Tensile strength (MPa)	Strain at break (%)
Neat PLA	2.92 ± 0.13	66.27 ± 1.70	3.52 ± 1.71
PLA/Fe_3O_4-5%	3.09 ± 0.05	57.94 ± 0.81	5.21 ± 2.33
PLA/Fe_3O_4-10%	3.16 ± 0.06	56.37 ± 0.08	3.62 ± 0.91
PLA/Fe_3O_4-15%	3.41 ± 0.06	55.48 ± 1.82	2.63 ± 0.22
PLA/Fe_3O_4-20%	3.53 ± 0.14	53.97 ± 1.04	2.22 ± 0.17
PLA/Fe_3O_4-25%	3.55 ± 0.07	52.28 ± 1.16	2.08 ± 0.14

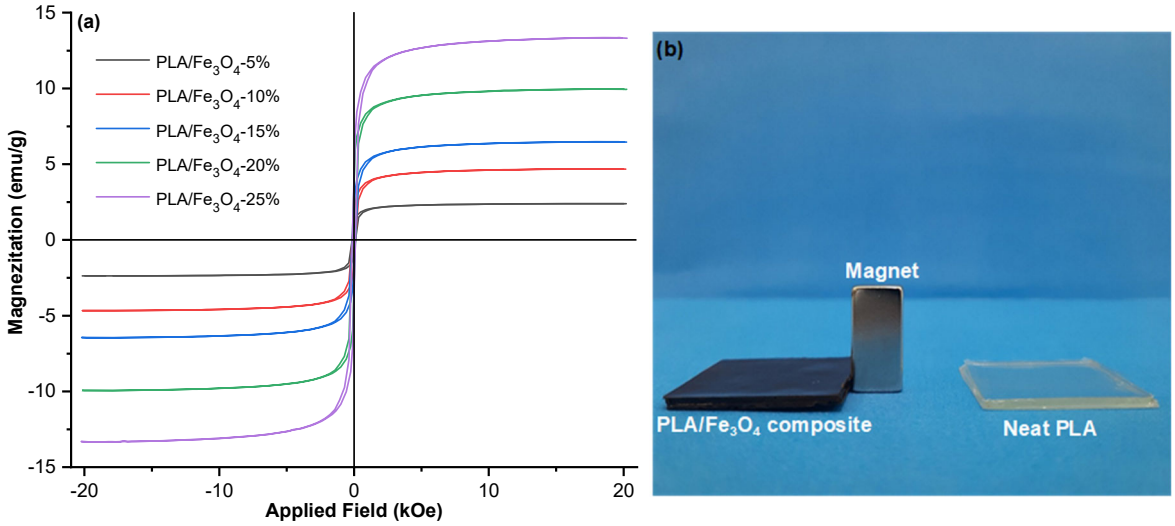

Fig 5. (a) Magnetic properties of PLA/Fe_3O_4 composites with a Fe_3O_4 content, (b) Comparison of magnet attraction by neat PLA and PLA/Fe_3O_4 composite

Table 4. Magnetic parameter of PLA/Fe_3O_4 composites

Samples	M_s (emu/g)	M_r (emu/g)	H_c (kOe)
Neat PLA	-	-	-
PLA/Fe_3O_4-5%	2.39	0.16	20.199
PLA/Fe_3O_4-10%	4.68	0.31	20.161
PLA/Fe_3O_4-15%	6.46	0.41	20.215
PLA/Fe_3O_4-20%	9.94	0.63	20.223
PLA/Fe_3O_4-25%	13.31	0.84	20.250

while PLA/Fe_3O_4 composite provides a magnetic response, as shown in Fig. 5(b).

The addition of 5 wt.% Fe_3O_4 into PLA resulted in magnetic properties of the PLA composite with a M_s of 2.39 emu/g and a M_r value of 0.16 emu/g (Table 4). The M_s and M_r values of the composite increased proportionally with the increase in Fe_3O_4 concentration. At 25 wt.% Fe_3O_4 content, the maximum M_s and M_r obtained were 13.31 and 0.84 emu/g, respectively. All composites' coercivity did not change significantly and remained almost constant with increasing Fe_3O_4 content. It shows that the coercive behavior is not controlled by the content of Fe_3O_4 particles but instead by the type of magnetic particles. The trend of increasing M_s and M_r due to the addition of magnetic filler is following previous studies [29].

Radar Absorption Performance of PLA/Fe_3O_4 Composite

The radar absorption performance of the samples is described by the RL value. Fig. 6 shows the RL curve of neat PLA and PLA/Fe_3O_4 composites, while the reflectivity, energy absorbed, and the position of the maximum absorption frequency is presented in Table 5. Although neat PLA resulted in an RL value of 5.17 dB, PLA is not categorized as a radar-absorbing material. The radar absorption value that appears from the neat PLA is perhaps due to the component of carbon atoms in PLA, trapped air, and sample thickness. However, when PLA was combined with Fe_3O_4 at the same thickness, the radar absorption behavior increased significantly as the Fe_3O_4 concentration increased. The addition of 5 wt% Fe_3O_4 improved the RL of PLA from –5.17 to –15.75 dB, with energy absorbed of 97.32% at frequency position 10.78 GHz. Furthermore, the RL of composites increased proportionally with the increase of Fe_3O_4 concentration. The composite at 25 wt.% Fe_3O_4 reached the highest RL of –25.83 dB, with energy absorbed 99.74% at 10.58 GHz and thickness of 3 mm.

As a magnetic loss absorber, the saturation magnetization of material will affect the radar absorption performance. The radar absorption intensity will grow as the saturation magnetization value increases. The addition of Fe_3O_4 magnetic material to PLA enhances the saturation magnetization of the composite, increasing the absorption performance of radar signals, as demonstrated in Tables 5 and 6. A comparison of the

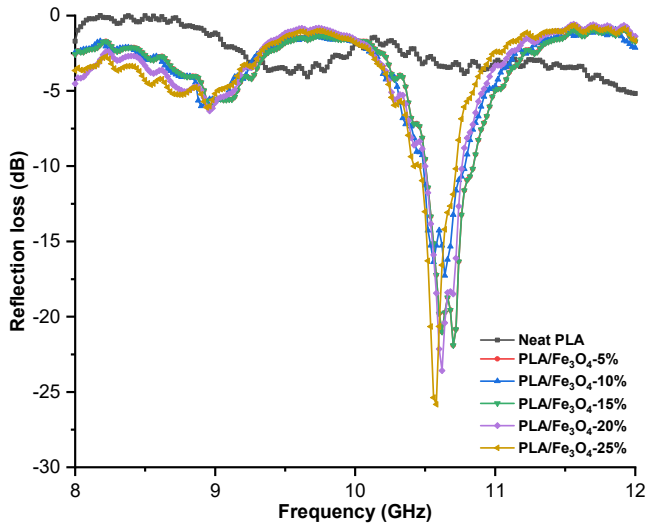

Fig 6. Radar absorption properties (thickness = 3 mm) of neat PLA and PLA/Fe_3O_4 composites. In set shows the zoom-out of the reflection loss graph at 10 to 11 GHz

reflectivity of composites of Fe_3O_4 in various polymer matrices is presented in Table 6. The RL value of the Fe_3O_4 in the PLA matrix is superior to other Fe_3O_4 composites. With a load of only 25 wt.% Fe_3O_4, PLA composite can absorb radar 72% higher than Poly(3,2-ethylenedioxythiophene) (PEDOT) composite at 80 wt.% Fe_3O_4 content. It can be concluded that the magnetic properties of Fe_3O_4 remained superior in the PLA polymer.

■ CONCLUSION

The radar absorption, thermal, and mechanical properties of PLA/Fe_3O_4 biocomposite have been successfully evaluated. The vector network analyzer measurements showed that the highest reflection loss of −25.83 dB occurred in PLA composites with a Fe_3O_4 concentration of 25 wt.%, about 399% higher than neat PLA. The TGA measurement revealed that Fe_3O_4 in various concentrations was able to maintain the thermal stability of neat PLA up to 280 °C. However, the decomposition temperature of all composites shifted to a lower temperature of neat PLA. The addition of 25 wt.% of Fe_3O_4 in PLA increased the tensile modulus of neat PLA from 2.92 to 3.55 GPa, while the tensile strength and the strain at the break did not change significantly. Based on these results, PLA/Fe_3O_4 biocomposites offer great promise in a wide range of radar absorption applications due to their good RL and thermo-mechanical properties.

Table 5. The reflectivity, energy absorbed, and the position of the maximum absorption frequency of neat PLA and PLA/Fe_3O_4 composites

Samples	Reflectivity (dB)	Energy absorbed (%)	Frequency position (GHz)
Neat PLA	−5.17	69.59	12.00
PLA/Fe_3O_4-5%	−15.72	97.32	10.66
PLA/Fe_3O_4-10%	−17.27	98.03	10.64
PLA/Fe_3O_4-15%	−21.90	99.35	10.70
PLA/Fe_3O_4-20%	−23.58	99.56	10.62
PLA/Fe_3O_4-25%	−25.83	99.74	10.58

Table 6. The reflectivity of Fe_3O_4 in various polymer matrices reported in several studies

Polymer matrix	Fe_3O_4 loading (wt.%)	Maximum absorption (dB)	Frequency position (GHz)	Thickness (mm)	Ref.
Poly(3,2-ethylenedioxythiophene (PEDOT)	80	−15	9	2.8	[30]
Polypyrrole	50	−22.4	12.9	2.3	[31]
divinylbenzene (DVB), and ethyl hexyl acrylate (EHA)	15	−23	9.3	3	[13]
Polyaniline	62.5	−24.7	14.8	2.0	[32]
Polyethylene	10	−24.3	9	4	[33]
PLA/Fe_3O_4-25%	25	−25.83	10.58	3	This work

■ ACKNOWLEDGMENTS

This study was supported by Research Center for Biomass and Bioproducts, National Research and Innovation Agency (BRIN), Indonesia. This work is also partly supported by the Ministry of Education, Culture, Research, and Technology of the Republic of Indonesia year 2021–2022 and the ITB research program in 2022. Rafles Sinaga gratefully acknowledges the financial support from *Lembaga Pengelola Dana Pendidikan* (LPDP), Ministry of Finance, Republic of Indonesia.

■ AUTHOR CONTRIBUTIONS

Rafles Sinaga conducted the conceptualization, data curation, formal analysis, investigation, methodology, and writing–original draft. Wida Banar Kusumaningrum conducted the conceptualization, investigation, project administration and resources. Yana Taryana conducted data curation, formal analysis, investigation, and methodology. Widya Fatriasari conducted a review, and formal analysis. Zuratul Ain Abdul Hami conducted a review, methodology, formal analysis. Holilah conducted formal analysis, investigation, methodology, and writing–original draft. Yudi Darma conducted conceptualization, supervision, and writing–original draft. Lisman Suryanegara conducted the conceptualization, data curation, formal analysis, funding acquisition, investigation; methodology, project administration, resources, supervision, and writing–original draft.

■ REFERENCES

[1] Wang, H., Xiu, X., Wang, Y., Xue, Q., Ju, W., Che, W., Liao, S., Jiang, H., Tang, M., Long, J., and Hu, J., 2020, Paper-based composites as a dual-functional material for ultralight broadband radar absorbing honeycombs, *Composites, Part B*, 202, 108378.

[2] Jayalakshmi, C.G., Inamdar, A., Anand, A., and Kandasubramanian, B., 2019, Polymer matrix composites as broadband radar absorbing structures for stealth aircrafts, *J. Appl. Polym. Sci.*, 136 (14), 47241.

[3] Liu, R., Miao, M., Li, Y., Zhang, J., Cao, S., and Feng, X., 2018, Ultrathin biomimetic polymeric $Ti_3C_2T_x$ MXene composite films for electromagnetic interference shielding, *ACS Appl. Mater. Interfaces*, 10 (51), 44787–44795.

[4] Saini, L., Gupta, V., Patra, M.K., Jani, R.K., Shukla, A., Kumar, N., and Dixit, A., 2021, Impedance engineered microwave absorption properties of Fe-Ni/C core-shell enabled rubber composites for X-band stealth applications, *J. Alloys Compd.*, 869, 159360.

[5] Adebayo, L.L., Soleimani, H., Yahya, N., Abbas, Z., Wahaab, F.A., Ayinla, R.T., and Ali, H., 2020, Recent advances in the development of Fe_3O_4-based microwave absorbing materials, *Ceram. Int.*, 46 (2), 1249–1268.

[6] Sambyal, P., Iqbal, A., Hong, J., Kim, H., Kim, M.K., Hong, S.M., Han, M., Gogotsi, Y., and Koo, C.M., 2019, Ultralight and mechanically robust $Ti_3C_2T_x$ hybrid aerogel reinforced by carbon nanotubes for electromagnetic interference shielding, *ACS Appl. Mater. Interfaces*, 11 (41), 38046–38054.

[7] Wu, N., Liu, C., Xu, D., Liu, J., Liu, W., Shao, Q., and Guo, Z., 2018, Enhanced electromagnetic wave absorption of three-dimensional porous Fe_3O_4/C composite flowers, *ACS Sustainable Chem. Eng.*, 6 (9), 12471–12480.

[8] Zhang, K., Zhang, Q., Gao, X., Chen, X., Wang, Y., Li, W., and Wu, J., 2018, Effect of absorbers' composition on the microwave absorbing performance of hollow Fe_3O_4 nanoparticles decorated CNTs/graphene/C composites, *J. Alloys Compd.*, 748, 706–716.

[9] Ni, S., Sun, X., Wang, X., Zhou, G., Yang, F., Wang, J., and He, D., 2010, Low temperature synthesis of Fe_3O_4 micro-spheres and its microwave absorption properties, *Mater. Chem. Phys.*, 124 (1), 353–358.

[10] Wang, G., Chang, Y., Wang, L., Liu, L., and Liu, C., 2013, Facilely preparation and microwave absorption properties of Fe_3O_4 nanoparticles, *Mater. Res. Bull.*, 48 (3), 1007–1012.

[11] Ni, S., Lin, S., Pan, Q., Yang, F., Huang, K., and He, D., 2009, Hydrothermal synthesis and microwave absorption properties of Fe_3O_4 nanocrystals, *J. Phys. D. Appl. Phys.*, 42, 055004.

[12] Li, Y., Li, X., Li, Q., Zhao, Y., and Wang, J., 2022,

Low-energy-consumption fabrication of porous TPU/graphene composites for high-performance microwave absorption and the influence of Fe_3O_4 incorporation, *J. Alloys Compd.*, 909, 164627.

[13] Phadtare, V.D., Parale, V.G., Lee, K.Y., Kim, T., Puri, V.R., and Park, H.H., 2019, Flexible and lightweight Fe_3O_4/polymer foam composites for microwave-absorption applications, *J. Alloys Compd.*, 805, 120–129.

[14] Jiang, S., Qian, K., Yu, K., Zhou, H., Weng, Y., and Zhang, Z., 2021, Study on ultralight and flexible Fe_3O_4/melamine derived carbon foam composites for high-efficiency microwave absorption, *Chem. Phys. Lett.*, 779, 138873.

[15] Murariu, M., and Dubois, P., 2016, PLA composites: From production to properties, *Adv. Drug Delivery Rev.*, 107, 17–46.

[16] Zhao, X., Liu, J., Li, J., Liang, X., Zhou, W., and Peng, S., 2022, Strategies and techniques for improving heat resistance and mechanical performances of poly(lactic acid) (PLA) biodegradable materials, *Int. J. Biol. Macromol.*, 218, 115–134.

[17] Suryanegara, L., Fatriasari, W., Zulfiana, D., Anita, S.H., Masruchin, N., Gutari, S., and Kemala, T., 2021, Novel antimicrobial bioplastic based on PLA-chitosan by addition of TiO_2 and ZnO, *J. Environ. Health Sci. Eng.*, 19 (1), 415–425.

[18] Valenzuela, R., Fuentes, M.C., Parra, C., Baeza, J., Duran, N., Sharma, S.K., Knobel, M., and Freer, J., 2009, Influence of stirring velocity on the synthesis of magnetite nanoparticles (Fe_3O_4) by the co-precipitation method, *J. Alloys Compd.*, 488 (1), 227–231.

[19] Qu, M., Wang, H., Chen, Q., Wu, L., Tang, P., Fan, M., Guo, Y., Fan, H., and Bin, Y., 2022, A thermally-electrically double-responsive polycaprolactone – thermoplastic polyurethane/multi-walled carbon nanotube fiber assisted with highly effective shape memory and strain sensing performance, *Chem. Eng. J.*, 427, 131648.

[20] Rezazadeh, N., Kianvash, A., and Palmeh, P., 2018, Microwave absorption properties of double-layer nanocomposites based on polypyrrole/natural rubber, *J. Appl. Polym. Sci.*, 135 (34), 46565.

[21] Bhattacharya, S., Roychowdhury, A., Das, D., and Nayar, S., 2015, Multi-functional biomimetic graphene induced transformation of Fe_3O_4 to ε-Fe_2O_3 at room temperature, *RSC Adv.*, 5 (109), 89488–89497.

[22] Yang, Y., Mao, X., Li, R., Zhang, M., Li, T., Wen, L., and Qin, L., 2022, Transformation of organonitrogen-encapsulated MOFs into N-doped Fe_3O_4@C nanopolyhedron via CVD super-assembly for photochemical oxidation, *Adv. Funct. Mater.*, 33 (3), 2210265.

[23] Koesnarpadi, S., Santosa, S.J., Siswanta, D., and Rusdiarso, B., 2017, Humic acid coated Fe_3O_4 nanoparticle for phenol sorption, *Indones. J. Chem.*, 17 (2), 274–283.

[24] Yu, B., Wang, M., Sun, H., Zhu, F., Han, J., and Bhat, G., 2017, Preparation and properties of poly (lactic acid)/magnetic Fe_3O_4 composites and nonwovens, *RSC Adv.*, 7 (66), 41929–41935.

[25] Barczewski, M., Hejna, A., Aniśko, J., Andrzejewski, J., Piasecki, A., Mysiukiewicz, O., Bąk, M., Gapiński, B., and Ortega, Z., 2022, Rotational molding of polylactide (PLA) composites filled with copper slag as a waste filler from metallurgical industry, *Polym. Test.*, 106, 107449.

[26] Barczewski, M., Mysiukiewicz, O., Matykiewicz, D., Skórczewska, K., Lewandowski, K., Andrzejewski, J., and Piasecki, A., 2020, Development of polylactide composites with improved thermomechanical properties by simultaneous use of basalt powder and a nucleating agent, *Polym. Compos.*, 41 (7), 2947–2957.

[27] Zhao, G., Liu, H.Y., Cui, X., Du, X., Zhou, H., Mai, Y.W., Jia, Y.Y., and Yan, W., 2022, Tensile properties of 3D-printed CNT-SGF reinforced PLA composites, *Compos. Sci. Technol.*, 230, 109333.

[28] Fan, W., Yuan, L., D'Souza, N., Xu, B., Dang, W., Xue, L., Li, J., Tonoy, C., and Sun, R., 2018, Enhanced mechanical and radar absorbing properties of carbon/glass fiber hybrid composites

with unique 3D orthogonal structure, *Polym. Test.*, 69, 71–79.

[29] Sukthavorn, K., Phengphon, N., Nootsuwan, N., Jantaratana, P., Veranitisagul, C., and Laobuthee, A., 2021, Effect of silane coupling on the properties of polylactic acid/barium ferrite magnetic composite filament for the 3D printing process, *J. Appl. Polym. Sci.*, 138 (38), 50965.

[30] Yan, L., Wang, X., Zhao, S., Li, Y., Gao, Z., Zhang, B., Cao, M., and Qin, Y., 2017, Highly efficient microwave absorption of magnetic nanospindle-conductive polymer hybrids by molecular layer deposition, *ACS Appl. Mater. Interfaces*, 9 (12), 11116–11125.

[31] Li, Y., Chen, G., Li, Q., Qiu, G., and Liu, X., 2011, Facile synthesis, magnetic and microwave absorption properties of Fe_3O_4/polypyrrole core/shell nanocomposite, *J. Alloys Compd.*, 509 (10), 4104–4107.

[32] Zhang, B., Du, Y., Zhang, P., Zhao, H., Kang, L., Han, X., and Xu, P., 2013, Microwave absorption enhancement of Fe_3O_4/polyaniline core/shell hybrid microspheres with controlled shell thickness, *J. Appl. Polym. Sci.*, 130 (3), 1909–1916.

[33] Ting, T.H., 2020, Synthesis, characterization of Fe_3O_4/polymer composites with stealth capabilities, *Results Phys.*, 16, 102975.